

# ASSESSING SDG 11.3.1 THROUGH MACHINE LEARNING-BASED CLASSIFICATION OF LANDSAT DATA AND DASYMETRIC POPULATION MAPPING: KENITRA CITY CASE STUDY

SAADANI MOUSSA<sup>1</sup>, ELBRIRCHI ELHASSAN<sup>2</sup>, BACHIR ALAMI OMAR<sup>3</sup>

<sup>1,2,3</sup> Geomatics Science Research Team (SGEO), LaGeS Laboratory, Hassania School of Public Works, Casablanca, Morocco,

E-mail : <sup>1</sup>moussa.saadani@gmail.com, <sup>2</sup>hbrirchi@yahoo.fr, <sup>3</sup>alami.ehtp@gmail.com

## ABSTRACT

In the current era, where the primary focus is on achieving sustainable urban development, the uncontrolled expansion of urban areas poses a substantial threat to their long-term sustainability. Within this context, Goal 11 of the Sustainable Development Goals (SDGs) assumes critical importance. This specific objective is dedicated to evaluating the sustainability of urban progress, with Indicator 11.3.1 serving as a central metric, measuring the "Ratio between the rate of land consumption and population growth." Faced with the need to quantify this indicator and recognizing the limitations inherent in traditional data sources, a shift toward non-conventional data becomes imperative. This transition to advanced methodologies is increasingly vital for a more accurate and comprehensive understanding of urban dynamics. The study focuses on a comprehensive assessment of SDG Indicator 11.3.1 in Kenitra city, spanning multiple time points (1994, 2004, 2014, and 2022). By utilizing Landsat imagery in conjunction with machine learning classifiers and Dasymetric population mapping, the research yields illuminating insights into the ratio of Land Consumption Rate to Population Growth—a crucial measure for assessing sustainable urbanization. From 1994 to 2004, this ratio stood at 2.64, indicating significant land consumption compared to population growth. Over the subsequent decade (2004-2014), the ratio decreased to 2.25, signifying a more balanced expansion trajectory. Particularly noteworthy is the period between 2014 and 2022, marked by a substantial decrease in the ratio to 0.68, reflecting a significant shift toward optimal land use. These findings highlight the dynamic evolution of urban development dynamics and the importance of strategic approaches for promoting sustainable urban growth.

**Keywords:** *Sustainable Development Goals, Landsat, Google Earth Engine, Machine Learning Classifiers, Dasymetric Population Mapping, Morocco, Kenitra*

## 1. INTRODUCTION

The adherence to the 2030 Agenda for Sustainable Development has engendered the imperative for a revolution in data compilation to scrutinize the multifaceted facets of SDGs Indicators encompassing economic, social, and environmental dimensions. This undertaking demands substantial exertion, particularly for the least developed countries that grapple with inadequacies in robust statistical infrastructure. This formidable challenge has galvanized reflection regarding alternative data sources, with a particular emphasis on those emanating from the paradigm-shifting Big Data revolution [1]. This paradigm shift holds the promise of elevating the data and statistical sources' potency,

capacitating statisticians to bridge extant lacunae and offer valuable insights for the oversight and documentation of sustainable development progress.

Morocco has undertaken substantial endeavors in the surveillance and tracing of Sustainable Development Goals indicators, manifesting through the formulation of annual reports and the establishment of an online platform to disseminate and expound upon SDG indicators. These initiatives adhere to internationally stipulated requisites and uphold open data standards [2], leveraging the data of the General Census of Housing and Population information, supplemented by an array of surveys spanning diverse economic, social, and demographic domains and encompassing

specific and representative samples. Yet, notwithstanding the concerted exertions, select indicators have remained not measured due to the limitations of conventional data sources. In light of this, our pursuit centers on the identification of indicators amenable to monitoring using Big Earth Data, subsequently, we seek develop a workflow to calculate them, delineating the methodologies and procedures for the computation of these indicators.

In light of the paramount significance attributed to the tenets of sustainable urban development, a distinct goal within the purview of the Sustainable Development Goals (SDGs) emerges - Goal 11. This goal manifests as a dedicated endeavor aimed at scrutinizing the sustainability of urban progress, particularly within cities and urban settlements. Among its sub-goals, Target 11.3 assumes prominence, directed towards the advancement of inclusive and sustainable urbanization. This entails fostering the capacity for participatory, integrated, and sustainable planning and management of human settlements, thus orchestrating a holistic vision of urban development [3]. Embedded within this strategic target is indicator 11.3.1: "Ratio of land consumption rate to population growth rate". Within the scope of this study, we undertook a comprehensive evaluation of this indicator, within the context of the Moroccan city of Kenitra over the time span spanning from 1994 to 2022. This endeavor was facilitated by taking advantage of Big Earth Data synergizing with the capabilities offered by Google Earth Engine. The essence of Indicator 11.3.1 resides in its assessment of urban land utilization efficiency, signifying the equilibrium attained between land consumption and population growth rates. Its significance rests upon the precision accorded to the identification of urban areas. As such, the realization of this metric hinges upon the accuracy in identifying and demarcating the urban spatial extent.

Sustainable urban development necessitates consistent and precise monitoring of urban expansion and population growth. This practice facilitates anticipatory and cohesive strategies for the orchestrated spatial and demographic progression of cities. Population growth signifies the escalation in service demand, underscoring the imperative to discern the spatial and temporal trajectories of urban expansion. This comprehension serves as the bedrock for interpreting trends and formulating responsive measures to address the requisites for essential services. Furthermore, this insight is instrumental in

safeguarding the ecological milieu, evidently, urban areas constitute one of principal variables instigating environmental shifts [4]. Moreover, urban planning is fundamental to the successful planning and management of public transport [5]. Consequently, a nuanced understanding of their spatial and temporal dynamics is essential not only for meeting basic service demands but also for preserving the equilibrium of the natural environment.

Prior to embarking upon the geographical delimitation of the urban area, a prerequisite step entails establishing precise criteria that defined urban extent independently of official administrative boundaries. This delineation is essential to demarcate the urban expanse distinctly from its peripheral surroundings [6]. Within our research endeavor, we chose to adopt the approach advocated by the UN-Habitat, centered on the concept of dynamic and functional city boundaries [7].

As previously discussed, Big Earth Data may play a pivotal role in monitoring certain SDGs indicators. Among the various forms of Big Earth Data, remote sensing emerges as a particularly potent avenue. Indeed, remote sensing imagery offers substantial potential in extracting pertinent insights concerning urban expansion [8]. For the purpose of this study, we employed imagery sourced from three distinct sensors: Landsat 5, Landsat 7, and Landsat 8. In our pursuit of pinpointing the urban area with utmost precision from medium-resolution remote sensing images, we opted to harness the capabilities of machine learning classifiers. It's noteworthy that machine learning classifiers have garnered substantial traction in recent times. Their widespread adoption is underscored by their exemplary accuracy and superior performance when contrasted with traditional parametric classifiers [8]. For our analysis we harnessed three machine learning classifiers, we subsequently conducted a comparative assessment of the outcomes, ultimately selecting the most accurate classifier. The classifiers employed encompassed Classification and Regression Trees (CART), Random Forest (RF) and Support Vector Machine (SVM). This approach enabled us to identify the classifier that exhibited optimal classification accuracy.

In addition, with the delimitation of the urban extent, we undertook the acquisition of detailed demographic datasets, spanning each annual interval under analysis from 1994 to 2022. Nevertheless, the acquired data exhibited partial alignment with our methodological requisites. We

therefore adopted an approach grounded in dasymetric population mapping [10]. This approach was underpinned by calibrated weights intricately linked to habitat classes. The overarching purpose of this technique was twofold: firstly, to ameliorate the inherent gaps within the demographic dataset, and secondly, to engender a spatial population grid commensurate in resolution with the urbanized area map.

The commitment of the Kingdom of Morocco to furthering the 2030 Agenda necessitates the establishment of integral mechanisms for measuring and monitoring the Sustainable Development Goals (SDGs) indicators, in particular the indicator 11.3.1. Unfortunately, this specific metric has yet to undergo official assessment at the national level, primarily due to the inadequacy of traditional data sources for its estimation.

The acquisition and dissemination of data pertaining to this indicator are not only critical for comprehending the complexities of urban growth dynamics but also for informing informed policies and strategic directions. Moreover, the significance of indicator 11.3.1 stems from its intricate interlinkages with numerous other SDG indicators, including 11.7.1 focusing on public space, 11.a.1 regarding regional development plans, 15.1.2 concerning forest space, 8.1.1 assessing annual GDP per capita growth, 8.5.2 linked to unemployment rates, and 11.6.1 associated with solid waste management.

A meticulous evaluation of this indicator ensures the comprehensive integration of broader spatial, demographic, and land dimensions, providing a foundational framework to achieve other objectives addressing poverty, health, education, energy, disparities, and climate change. Thus, acknowledging the significant importance of this undertaking, the formulation of a comprehensive methodology for assessing this indicator within the unique Moroccan context is imperative, alongside the validation of this approach in a real-world setting, such as the city of Kenitra.

The intrinsic value of this research effort resides in its endeavor to address the data gaps. This translates into employing methodologies specifically tailored to address the gaps and inadequacies found within the datasets, aligning closely with the nuances of the Moroccan context. These methodologies involve exploring innovative approaches and utilizing alternative data sources to supplement the missing information. By adeptly navigating and

resolving these gaps, this research aspires to fortify the reliability and precision of the derived outcomes, thereby presenting a more holistic and precise depiction of the subject under study.

In summary, our research diligently adhered to a methodology aligned with UN-Habitat guidelines, comprising distinct phases. Initially, we delineated the analysis timeframe, selecting the study area based on its national significance and pronounced urban and demographic evolution. Subsequently, utilizing remote sensing imagery, we computed the land consumption rate following the adopted urban area definition, while also calculating the population growth rate. The culmination of our approach involved the derivation of the Land Consumption Rate to Population Growth Rate (LCRPGR) and the computation of prescribed secondary metrics.

## 2. STUDY AREA

The area of our study, as illustrated in Figure 1, encompasses both the Moroccan city of Kenitra and the Mehdyia district, functioning as a seamless urban extension of Kenitra. Positioned approximately forty kilometers north of Rabat, this locale resides upon an elevated plateau, affording an expansive view of the wadi Sebou as it forms a sweeping arc in proximity to its estuarine outlet. Kenitra is situated inland from a coastal configuration defined by a cordon dune formation, beneath which a mosaic of lakes and plains, particularly prominent in the northern sector, comes into view.

To the southern periphery of the city lies the expansive Maamora forest, renowned as Morocco's largest cork forest. Situated within a broader context, the urban cluster occupies a strategic position at the juncture of the northern plain (Gharb) and the fertile Sebou basin (Saïss), which are characterized by their agricultural abundance. Moreover, the city is situated at the northern extremity of the Casablanca-Rabat coastal metropolitan area—a nexus of concentrated populations, essential services, industrial establishments, and vital infrastructure. Kenitra's robust connectivity with these domains is facilitated by a robust network of high-quality motorways, roadways, and rail systems.

Kenitra constitutes an urban agglomeration currently undergoing significant structural evolution due to pronounced demographic expansion. Furthermore, its trajectory is characterized by rapid

advancement, propelled by an array of residential initiatives and large-scale undertakings. This dynamic urban development is further facilitated by a robust network of infrastructure and essential facilities, which contribute substantively to Kenitra's burgeoning landscape.

The selection of Kenitra as our study area is underpinned by its engagement in a series of prominent and pivotal projects over recent years. Moreover, the city has witnessed substantial demographic expansion, further accentuating its significance within our research framework.

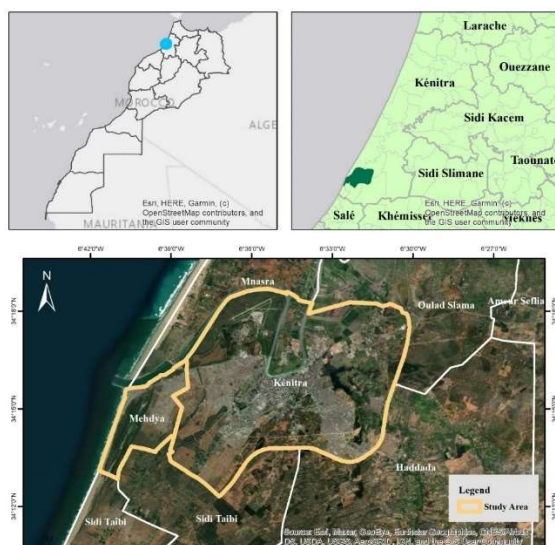


Figure 1. Study area: location of Kenitra City in Morocco

### 3. DATA AND METHODOLOGY

#### 3.1. Identification of urban areas

##### 3.1.1. Data

To delineate the urban area, we utilized imagery from three different sensors: Landsat 5, Landsat 7, and Landsat 8. These images were corrected for atmospheric reflectance effects, and any discrepancies caused by the satellite sensors. Utilizing the powerful capabilities of Google Earth Engine (GEE), we accessed a comprehensive and freely available collection of Landsat image series, boasting an average resolution of 30 meters.

Leveraging supervised classification entailed the meticulous acquisition of accurate data to ensure the optimal calibration of our classification algorithms. To accomplish this, we meticulously generated data through visual interpretation of the available images. The assessment of outcomes

followed a comprehensive methodology, amalgamating the maps provided with demographic data and visual interpretations.

#### 3.1.2. Image classification

To achieve a precise classification, we employed multiple classifiers and subsequently conducted a comparative analysis of their outcomes. These classifiers can be classified into two categories: parametric classifiers, which involve evaluating each pixel individually and assigning the thematic class based on its color. Numerous parametric classifiers are available, including the Maximum Likelihood Classifier. Until approximately a decade ago, this classifier served as the benchmark algorithm for image classification due to its remarkable classification accuracy [11]. Non-parametric classifiers, on the other hand, entail partitioning the image into coherent segments and subsequently assigning the appropriate thematic class to each segment. Homogeneity criteria for segments may encompass factors such as color, shape, size, texture, and spatial positioning. Within the realm of non-parametric classification techniques, Machine Learning emerges as a dependable approach. In recent times, the field of remote sensing has witnessed a burgeoning adoption of machine learning for novel classification techniques. This shift underscores the growing reliance of remote sensing scientists on the potential of machine learning to enhance classification methodologies [12].

A majority of studies undertaken to scrutinize and contrast non-parametric classifiers have been confined to distinct study areas and topographical features, each involving specific datasets [13], [14], [15]. Consequently, it was impractical to extrapolate the findings from these comparative studies directly onto our study region. In light of this limitation, our strategy encompassed the utilization of three distinct machine learning-based classifiers. The subsequent comparative analysis allowed us to select the most adept classifier based on classification accuracy. These classifiers include Classification and Regression Trees (CART), Random Forest (RF), and Support Vector Machine (SVM). Notably, all of these classifiers are accessible within the GEE online cloud computing platform, enhancing the feasibility of our methodology.

In addition to the inherent spectral bands (Blue, Green, Red, Near Infrared, SWIR 1, SWIR 2), supplementary bands were generated for input into

the classification algorithms. These additional bands were derived from the Enhanced Vegetation Index (EVI) [16] and Soil-Adjusted Vegetation Index (SAVI) [17] spectral indices, as outlined in Table 1.

Table 1. Spectral indices calculated for optical Landsat imagery

Index	Calculation
EVI	$2.5 * \frac{NIR - RED}{NIR + 6 * RED - 7.5 * BLUE + 1}$ (1)
SAVI	$1.5 * \frac{NIR - RED}{NIR + RED + 5000}$ (2)

The precision of the classification hinges on the quality of the training samples utilized. Hence, as illustrated in Figure 2 we designed a semi-random sampling approach that amalgamates probabilistic elements with a systematic framework. Referred to as framed random sampling, this strategy harmonizes randomness and structured design to attain optimal sample selection. By adopting this approach, we mitigate potential bias, thus elevating the accuracy of our classifications.

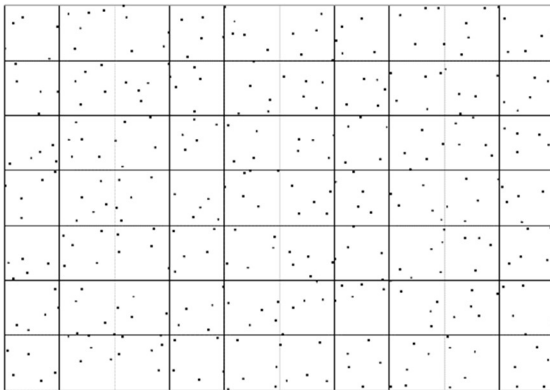


Figure 2. Illustration of the training sample constructed using a semi-random sampling strategy, based on a probabilistic character and guided by a grid.

Once the sample points had been selected, we set about identifying the class assigned to each point in the sample, based on a visual interpretation of the original images and reference maps. Initially, we conducted a classification of the images into five distinct classes, namely Built-Up, Cropland, Baren, Forest, and Water Bodies. As we employed a semi-randomized strategy guided by a grid-based framework, this strategy ensured that all classes were duly represented in the sample set, proportionate to their actual sizes within the analyzed area.

With our primary objective centered around the identification of built-up areas, we amalgamate

all classes other than built-up into a unified class denoted as Non-Built-Up. Subsequently, the accuracy assessment was conducted based on the classification of two overarching classes: Built-Up and Non-Built-Up.

Figure 3 offers a comprehensive depiction of the primary methodology adopted for the classification and extraction of built-up areas. This entire procedure was executed within the collaborative environment of the Google Earth Engine (GEE) platform and the QGIS Desktop software.

### 3.1.3. Accuracy Assessment

Validation of the classification results is also tested on a sample selected using a semi-random strategy. The correlation analysis between the classification results and the reference data is carried out using an approach based on a pixel-by-pixel comparison.

With regard to the performance metrics chosen for validation, we opted for metrics derived from the confusion matrix [18]. These include the kappa coefficient K, as well as the errors of commission C and omission O, as defined by equations (3), (4) and (5). These performance indicators provide valuable information about the accuracy of the classification.

$$K = \frac{P_o - P_e}{1 - P_e} \quad (3)$$

$$C = \frac{FP}{TP+FP} \quad (4)$$

$$O = \frac{FN}{TP+FN} \quad (5)$$

Where the labels TP (True Positive), TN (True Negative), FP (False Positive), and FN (False Negative) refer to the elements of the confusion matrix, while:

$$P_o = \frac{TP+TN}{TP+FP+FN+TN} \quad (6)$$

and

$$P_e = \frac{(TP+FN)(TP+FP)+(FP+TN)(FN+TN)}{(TP+FP+FN+TN)^2} \quad (7)$$

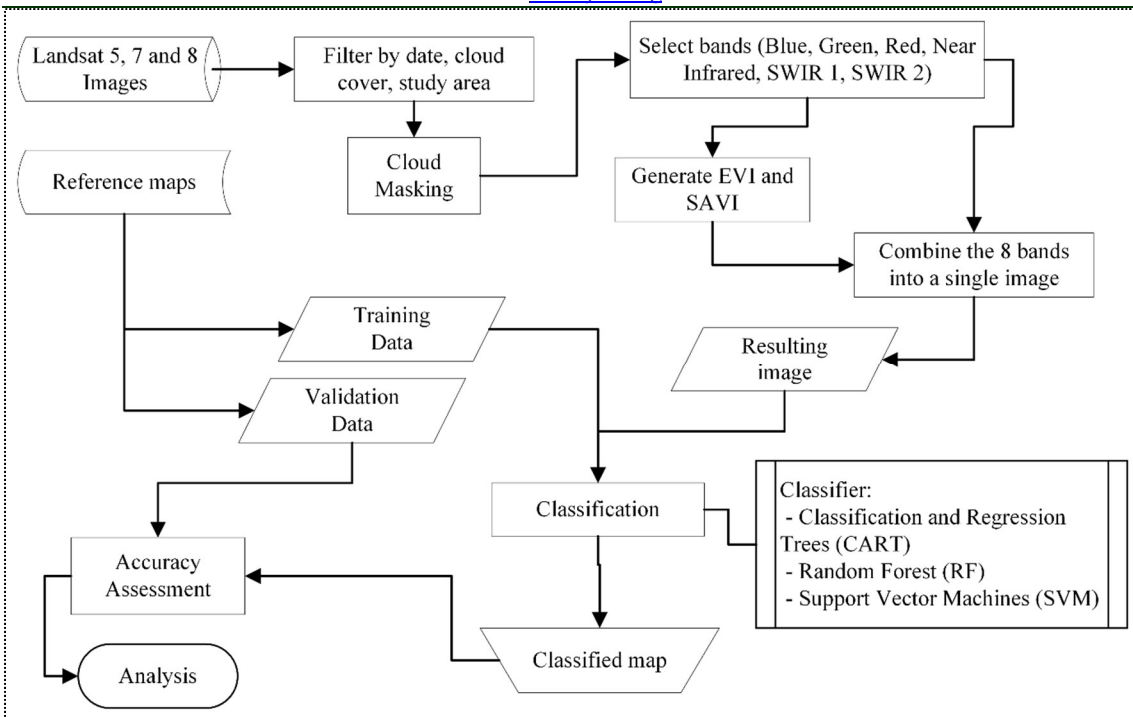


Figure 3. The overall classification methodology

$P_o$  represents the overall accuracy, providing information about the proportion of correct classifications for all the pixels in a specific site. It is a measure of how well the classifier performs in correctly identifying the true positive and true negative samples.

### 3.1.4. Urban area definition

As outlined in the Metadata of Indicator 11.3.1 [19], its primary objective revolves around assessing the interplay between urban area transformation and population growth across temporal dimensions. Thus, the foremost consideration for generating precise and representative estimates for this indicator pertains to the definition of the urban area itself. Importantly, the urban extent is not invariably bound by existing municipal confines; rather, it's contingent on diverse approaches based on individual countries' urban planning and demographic attributes.

In our study, we aligned with the UN-Habitat's perspective. Here, an urban area signifies a region that manifests urban characteristics spatially, functionally, or through intrinsic urban attributes. This approach acknowledges urban domains as dynamic entities subject to fluctuation, poised to expand or contract due to diverse influences, rather than being rigidly circumscribed within fixed

parameters. In essence, it embodies the concept of dynamic and functionally evolving urban boundaries.

For the precise delineation of the city's functional and dynamic boundaries, we executed a classification of the built-up area employing Landsat imagery. This classification encompasses three distinct categories: urban, suburban, and rural. The classification criterion hinges on an assessment of pixel contextual features within their surrounding environment. This approach is aligned with the methodology endorsed in the Atlas of Urban Expansion, a collaborative initiative between The NYU Urban Expansion Program and UN-Habitat [20], [21].

The classification methodology hinges on the density of built-up pixels encompassed within a spatial radius, referred to as a walking distance circle, which spans an area of one square kilometer with a radius of approximately 564 meters—equivalent to approximately a ten-minute walk. Within this context, a pixel's classification is contingent on its position within this circle. Precisely, if the proportion of built-up pixels within the circle surpasses 50%, the pixel is designated as urban. A pixel falls within the suburban category if the density of built-up pixels within the circle ranges from 25% to 50%. Conversely, pixels registering a

density below 25% for built-up pixels within the circle are categorized as rural (Figure 4)

The boundaries of the city obviously include not only built-up pixels, but also other undeveloped areas within and surrounding built-up areas. We have included non-built-up pixels in the city boundary in the following cases:

- ✓ Fringe undeveloped areas: All non-built-up pixels located within 100 meters of urban or suburban pixels.
- ✓ Captured undeveloped areas: All non-built-up pixels clusters that are completely surrounded by urban and suburban built-up pixels, along with the undeveloped areas surrounding them. These clusters must have an area of less than 200 hectares.

The delimitation of the city boundaries, according to the methodology described above, was developed and implemented using the capabilities offered by the QGIS software. This process was carried out after downloading the land use maps that we produced using GEE (Google Earth Engine).

### 3.2. Population growth rate

#### 3.2.1. Demographic data

In Morocco, population data is provided by the High Commission for Planning (HCP) in the context of the General Census of Population and Housing (GCPH). The HCP aggregates population statistics into areal units such as control sectors, which are homogeneous in size, with an approximate average of 450 households. Or according to the administrative subdivision, which the smallest unit is the commune, with sizes ranging from a few thousand to several hundred thousand. Precisely, the

HCP divides the territory into census districts with an average size of 150 households. These districts are used for the HCP's internal needs as well as for sampling and for drawing up survey plans and carrying out the various surveys, but for reasons of anonymity of responses and protection of personal data, the demographic data aggregated into districts is not accessible either to the public or to consultancy firms or research centers. The HCP has aggregated these data into control sectors, each sector representing three districts.

#### 3.2.2. Dasymetric population mapping

Despite the very fine statistical segmentation according to control sectors, it does not allow high-resolution population grid estimates to be obtained. Although this sectoral aggregation facilitates sampling conception and guarantees the anonymity of responses, it can also lead to inference problems when attempting to generate a high-resolution population grid. By way of illustration, sectors located in city centers are characterized by their relative smallness and a homogeneous distribution of their inhabitants, whereas units in suburban areas are larger and display a non-uniform population distribution. This leads to a problem linked to the mutability of geographical units, which makes census data unsuitable for accurately projecting population density and distribution, particularly in suburban or semi-urban areas.

Several approaches have been developed with the aim of generating gridded demographic data by overcoming the pitfalls of aggregated national census data [22], [23].

These approaches are based on the assumption that the land use map is a powerful

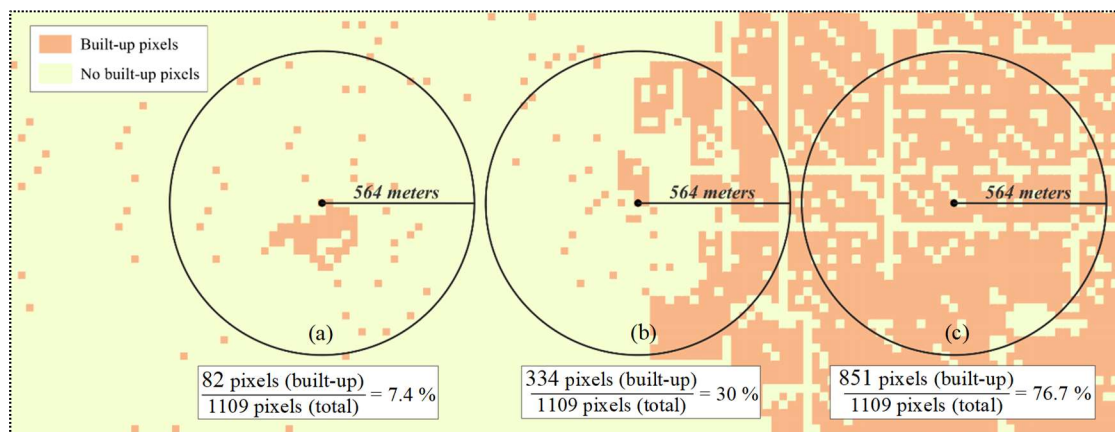


Figure 4. Illustrating The Concept Of Identifying Urban Areas Based On The Density Of Built-Up Pixels Within A Walking Distance Circle; A. Rural Pixel, B. Suburban Pixel, C. Urban Pixel

predictor of population distribution [24]. Using this map as a reference, dasymetric mapping can be used to disaggregate coarse resolution population estimates to produce a finer resolution estimate of population distribution [10], [21].

In this study, we have opted for the use of dasymetric mapping based on an intuitive approach which consists of applying an empirical relationship defining population weights, producing a population map per 30 m grid cell for the study area. To generate the map, we use publicly available population data from the HCP for the years 1994, 2004, 2014 and 2022 disaggregated by commune, and 2014 population data disaggregated by control sectors, in combination with built-up area map with a resolution of 30 meters developed as part of this study. In our approach, we assigned a population value of zero to all the pixels corresponding to non- built-up areas. We then distributed the population of each commune or control sector between the remaining pixels corresponding to built-up areas and according to weighting classes based on the dominant habitat type. Indeed, as previously noted, the control sectors are homogeneous in terms of habitat type. In fact, the control sectors are classified into seven distinct categories according to the predominant habitat type, namely “Luxury Housing”, “Modern Housing”, “Traditional Housing”, “Medium Collective Housing”, “Economically and Socially Housing”, “Informal and Basic Housing” and “Rural Dwelling”.

This classification provided us with valuable information for refining the quality of the dasymetric population mapping, especially in years when we do not have disaggregated population data. We used this information on housing types to create weighting classes. Each weighting class represents a relative weight assigned to the population of a control sector based on the dominant habitat type. Using these weighting classes, we were able to refine the quality of the dasymetric population mapping. The weights assigned to each control sector were used to distribute the population more precisely between the pixels corresponding to the built-up areas. In this way, the representation of the population in the dasymetric mapping was adjusted to better reflect the actual distribution of the population according to the different habitat types. This approach of using weighting classes based on habitat type helps to improve the accuracy and reliability of dasymetric population mapping. It better captures small-scale demographic variations

and provides more detailed information on the distribution of the population in the study area.

It is important to note that the 30-metre resolution of the built-up areas map was also used as the basis for the dasymetric population map. This has enabled us to maintain spatial consistency and ensure that the population information is aligned with the identified built-up areas.

### 3.2.3. Estimation of Weighting for Habitat Classes

As mentioned previously, the population data aggregated by sector for the year 2014 are homogeneous in terms of habitat types. For the other years, the population data is aggregated by commune. To optimally assign the population sizes according to habitat classes, we calculated the population weights for each habitat class, using 2014 as the reference year. This was performed using the following steps.

Firstly, we estimate the weighting classes as appropriate to the reference year:

$$W_{r_h} = \frac{Pr_h}{Ar_h} \quad (8)$$

Where  $Ar_h$  the total surface of the built-up area of habitat class  $h$ ,  $Pr_h$  the total number of populations living in the zone with habitat class  $h$ , and  $W_{r_h}$  the weighting coefficient for habitat class  $h$ .

Then, using the reference weighting classes, we estimate the weighting classes for the year of estimation.

$$W_{e_h} = W_{r_h} * \frac{Pt_e}{Pt_{er}} \quad (9)$$

Where:

$W_{e_h}$  The Weighting coefficient for habitat class  $h$  for the estimation year,  $Pt_e$  The total population of the year of estimation and  $Pt_{er}$  The estimated total population calculated using the weighting classes for the reference year, calculated according to the formula

$$Pt_{er} = \sum_{h=0}^n W_{r_h} * Pr_h \quad (10)$$

Where  $n$  is the number of habitat classes

### 3.3. Indicators computation

The primary metric utilized in SDG 11.3.1 indicator pertains to the proportion between the rate of land consumption and the rate of population growth, denoted as the Land Consumption Rate to Population Growth Rate (LCRPGR). This metric quantifies the annual expansion of urban areas relative to the annual increase in population over a specific timeframe [7]. It is important to acknowledge that a LCRPGR value below 1 indicates that the population growth rate exceeds the rate of land use during the specified period. A value of 1 signifies an equilibrium, where the rates of population increase and land consumption are equivalent. Conversely, a LCRPGR value exceeding 1 suggests that the annual rate of land depletion surpasses the rate of population growth. Nonetheless, this explanation of the indicator fails to indicate the threshold at which cities become excessively crowded or sparsely populated, nor does it account for negative growth [25], [26].

Given the aforementioned constraints associated with the LCRPGR metric, alternative significant descriptive measures such as per capita land consumption and the percentage variation in built-up area have been put forth for consideration in relation to indicator 11.3.1.

Per capita land use scrutinizes the extent of spatial utilization attributed to each individual within a given urban context. It is crucial to highlight that certain scholars regard this measure as a more significant indicator for assessing land consumption compared to the LCRPGR, primarily due to its

ability to elucidate intra-city transformations and dynamics.

Within the purview of this study, we conducted calculations pertaining to per capita land use under absolute circumstances. This involved the division of the aggregate built-up area within the defined urban boundaries during a specific year by the corresponding population associated with that spatial domain.

The formulation for the computation of the LCRPGR metric adheres to the metadata standards endorsed by the United Nations, while the formulas utilized to estimate the remaining two indicators are recommended by UN-Habitat [27]. Table 2 shows the formulas used for these metrics.

## 4. RESULTS AND DISCUSSION

### 4.1. Urban areas

#### 4.1.1. Classification

In pursuit of achieving a more refined classification, we employed three different classifiers based on machine learning. These classifiers include Classification and Regression Trees (CART), Random Forest (RF) and Support Vector Machine (SVM). The Table 3 exhibits the outcomes yielded by each classifier, illustrating the classification results obtained across all the years under analysis.

Table 2. Indicator computation formulas

Metric	Formula	Symbol Explanation
Land Consumption Rate (LCR)	$\frac{V_{\text{present}} - V_{\text{past}}}{V_{\text{past}}} * \frac{1}{(t)}$	$V_{\text{present}}$ is total built-up area in current year $V_{\text{past}}$ is total built-up area in past year $t$ is the number of years between $V_{\text{present}}$ and $V_{\text{past}}$ (or length in years of the period considered)
Population Growth rate (PGR)	$\frac{\text{LN}(\text{Pop}_{t+n}/\text{Pop}_t)}{(y)}$	$\text{LN}$ is the natural logarithm value $\text{Pop}_t$ is the total population within the urban area/city in the past/initial year $\text{Pop}_{t+n}$ is the total population within the urban area/city in the current/final year $y$ is the number of years between the two measurement periods
LCRPGR	LCR/PGR	
Built-up area per capita (m <sup>2</sup> /person)	$\left(\frac{\text{UrBU}_t}{\text{Pop}_t}\right)$	$\text{UrBU}_t$ is the total built-up area/city in the urban area in time $t$ (in square meters) $\text{Pop}_t$ is the population in the urban area in time $t$
Total change in built up area (%)	$\frac{(\text{UrBU}_{t+n} - \text{UrBU}_t)}{\text{UrBU}_t}$	$\text{UrBU}_{t+n}$ is the total built-up area in the urban area/city in time the current/final year $\text{UrBU}_t$ is the total built-up area in the urban area/city in time the past/initial year

Table 3. The Classification Outcomes Of Built-Up And Non-Built-Up Land Cover Classes Derived From Landsat 5, 7, And 8 Using CART, RF, And SVM Classifiers Over The City Of Kenitra

	Landsat	CART	RF	SVM
2022				
2014				
2004				
1994				

As illustrated in the Figure 5 and indicated in Table 4 examination of the four distinct performance metrics demonstrates that the Random Forest classifier exhibited superior values of overall

accuracy and kappa, alongside minimal commission and omission error. This exemplary performance remained consistent throughout all years of analysis;

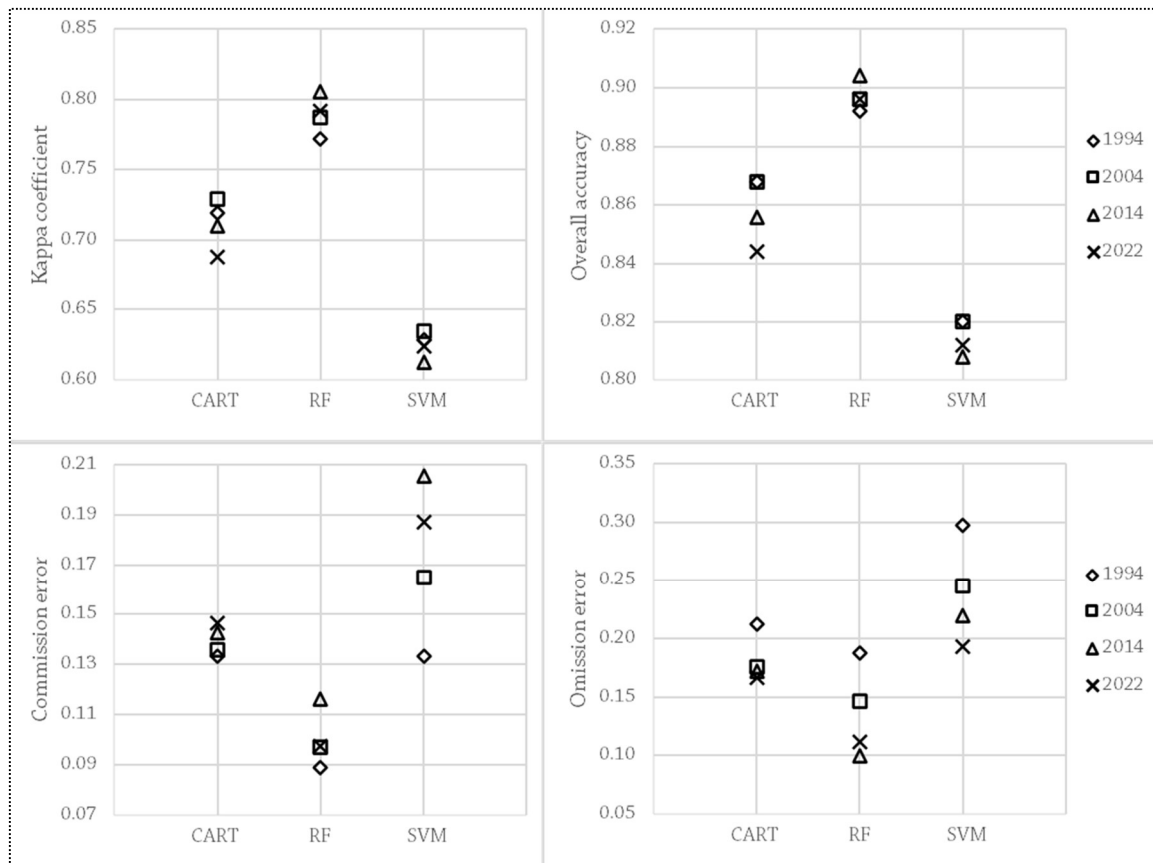


Figure 5. Performance Metrics For Selected Classifiers

Table 4. Accuracy Assessment Results, Where K: Kappa Coefficient; C: Commission Error, O: Omission Error And P<sub>o</sub>: The Overall Accuracy,

	Testing sample size (No. of Pixels)			CART				RF				SVM			
	Total	Built-Up	Non-Built-Up	C	O	P <sub>o</sub>	K	C	O	P <sub>o</sub>	K	C	O	P <sub>o</sub>	K
1994	250	90	160	0.13	0.21	0.87	0.72	0.09	0.19	0.89	0.77	0.13	0.30	0.82	0.63
2004	250	103	147	0.14	0.18	0.87	0.73	0.10	0.15	0.90	0.79	0.17	0.25	0.82	0.63
2014	250	112	138	0.14	0.17	0.86	0.71	0.12	0.10	0.90	0.81	0.21	0.22	0.81	0.61
2022	250	123	127	0.15	0.17	0.84	0.69	0.10	0.11	0.90	0.79	0.19	0.19	0.81	0.62

In view of these outcomes, we opted to lean upon the classified maps derived through the RF classifier. Consequently, all subsequent analyses are predicated upon this map. The selection of the Random Forest classifier following this comparative assessment provided augmented assurance in the caliber and dependability of the attained results, thereby enabling us to deduce more resilient and insightful inferences within the ambit of our study.

4.1.2. Urban area delimitation

Following the extraction of built-up areas, we proceeded to delineate the urban area according to the methodological framework adopted in this research.

The findings reveal a profound evolution of urban expansion delineated by functional city boundaries, characterized by substantial modifications spanning each analytical interval, as depicted on Figure 6 evidently, this cartographic representation attests to the convergence of the municipalities of Kenitra and Mehdiya, ultimately resulting in an amalgamated entity.

The specifics of this urban expansion are comprehensively delineated within

Figure 7 and Table 5, as the latter lucidly exemplifies, the tempo of development between built-up areas and urban extent harmoniously aligns.

The results unveil an upward trajectory in the expansion of built-up areas within the study zone. In 1994, the built-up area within the study zone covered 17.27 km<sup>2</sup>. Over the ensuing years, this metric experienced a notable augmentation, culminating at 47.23 km<sup>2</sup> by the year 2022. This tangible surge in built-up spaces closely mirrors the trajectory of urban development.

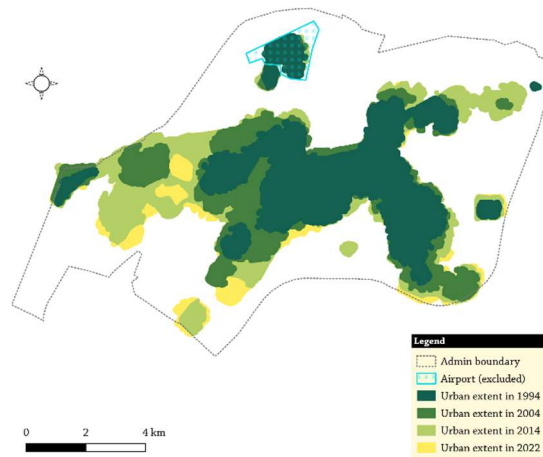


Figure 6. Urban Extent Evolution Spanning The Years 1994 To 2022

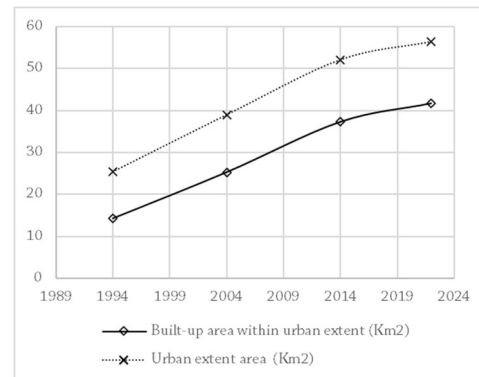


Figure 7. Tempo Of Development Between Built-Up Areas And Urban Extent Spanning The Years 1994 To 2022

If we narrow our focus solely to the assessment of the built-up area within the urban extent, as defined by the functional limits of the city. The results illustrate that the built-up area within this defined extent expanded from 14.29 km<sup>2</sup> in 1994 to 41.66 km<sup>2</sup> in 2022. This delineates a substantial

transformation, underlining the city's marked expansion over time. datasets, we ascertained that the overall accuracy of these findings surmounts the threshold of 90%.

Table 5. Built-up area within urban extent and Urban extent area evolution spanning the years 1994 to 2022

Years of analysis	Built-up area within the study zone		Built-up area within urban extent		Urban extent area (Km <sup>2</sup> )
	No. of Pixels	Built-up area (Km <sup>2</sup> )	No. of Pixels	Built-up area (Km <sup>2</sup> )	
1994	19192	17.27	15877	14.29	25.46
2004	32468	29.22	28095	25.29	39.02
2014	47111	42.40	41397	37.26	52.14
2022	52482	47.23	46293	41.66	56.45

#### 4.2. Demographic metrics

Following the delineation of built-up areas and the delineation of urban expansion based on the city's functional boundaries, we embarked on the identification and computation of demographic metrics employing dasymetric mapping techniques for population distribution and habitat categorizations.

##### 4.2.1. Habitat Classes Weighting

Establishing the weightings constituted a crucial stride in drawing up the dasymetric population mapping. As illustrated in Figure 8 and detailed in Table 6 an observable decline prevails in the weights, a phenomenon explicable through two paramount factors. The initial causative element correlates with the reduction in the average size of households, dwindling from 5.5 in 1994 to 4.1 in 2014 [28], [29]. The secondary determinant derives from endeavors geared towards the urban fabric's restructuring, coupled with initiatives to counteract the proliferation of shantytowns and ad hoc housing settlements.

Unfortunately, an adequate corpus of data across all timeframes was lacking to substantiate and gauge the veracity of these outcomes comprehensively. Nevertheless, we managed to acquire a circumscribed subset of finely dissected demographic data pertaining to the year 2004. Upon juxtaposing the inferred outcomes with these

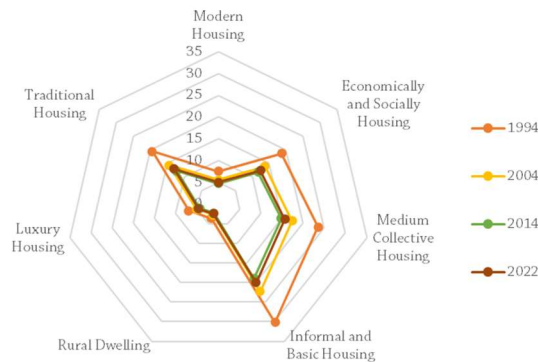


Figure 8. Shifts In Weighting Of Habitat Classes Over The Years

##### 4.2.2. Population within the city's functional limit

The predominant input data for indicator 11.3.1 is the number of inhabitants. This metric is computed at this juncture employing the dasymetric mapping approach, predicated upon the weightings calculated in the antecedent step, Hence, we assessed the population residing within the city's functional boundaries. The outcomes are delineated in Table 7.

Table 6. Estimated Weighting Of Habitat Classes

Habitat Classes	Habitat Classes Weighting			
	1994	2004	2014 (The reference year)	2022
Modern Housing	7.48	5.53	4.72	4.97
Economically and Socially Housing	18.68	13.79	11.77	12.42
Medium Collective Housing	23.59	17.42	14.87	15.68
Informal and Basic Housing	30.18	22.28	19.01	20.06
Rural Dwelling	3.68	2.71	2.32	2.44
Luxury Housing	7.00	5.17	4.41	4.65
Traditional Housing	19.45	14.36	12.26	12.93

Table 7. Approximated Population Within The City's Functional Limits

Population	Years of analysis			
	1994	2004	2014	2022
Population within administrative limits	298532	368316	452526	528875
<b>Approximated Population Within the city's functional limits</b>	<b>249554</b>	<b>334209</b>	<b>412389</b>	<b>490571</b>

### 4.3. Metrics for SDG 11.3.1 Indicator

The metrics emanating from indicator ODD 11.3.1 have unveiled intricate interrelationships between urban development and population dynamics throughout the studied timeframe. through an analytical review of the outcomes elucidated in Table 8 and Figure 9, we notice that the period spanning from 1994 to 2004 witnessed significant urban expansion, with an absolute increase of built-up area by 11 km<sup>2</sup>, representing a remarkable 76.98% total change. The rate of land consumption during this decade was notably high, at +0.077. Concurrently, the population size grew by 84655 individuals, indicating a population growth rate of +0.029 and a Land Consumption Rate Population Growth Ratio (LCRPGR) of 2.64.

Transitioning to the subsequent decade, from 2004 to 2014, the built-up area experienced a further increase of 11.97 km<sup>2</sup>, accounting for a total change of 47.33%. The land consumption rate exhibited a relatively moderate increment at +0.047. The population grew by 78180, with a population growth rate of +0.021. The LCRPGR for this period was 2.25, indicating a continued alignment between land consumption and population growth.

Examining the most recent period, from 2014 to 2022, the expansion of built-up areas became more restrained, with an absolute rise of 4.40 km<sup>2</sup> and a total change of 11.81%. The land

consumption rate decreased to +0.015, reflecting a more controlled urban expansion pattern. Notably, the population size grew by a comparable figure of 78182, reflecting a population growth rate of +0.022. The LCRPGR for this phase notably diminished to 0.68, indicative of a more sustainable balance between land consumption and population growth.

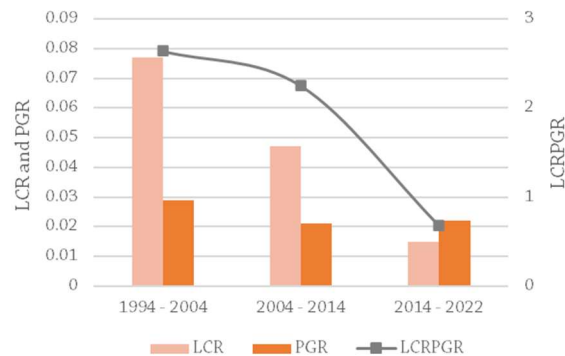


Figure 9. Land Consumption Rate To Population Growth Rate Trend Throughout The Studied Timeframe

In tandem with the primary metrics outlined earlier, there exists an additional secondary metric: Built-up area per capita (m<sup>2</sup>/person). Figure 10 encapsulates the outcomes pertaining to this supplementary measure. This figure illustrates the evolving interplay between urban expansion and population distribution. it's evident that the relationship between urbanization and spatial availability is dynamic. Beginning at 57.26 m<sup>2</sup>/person in 1994, the metric grows steadily to 75.67 m<sup>2</sup>/person in 2004, emphasizing urban sprawl. By 2014, it reaches 90.35 m<sup>2</sup>/person, reflecting evolving urban patterns. In 2022, it slightly decreases to 84.92 m<sup>2</sup>/person, it may signify refined spatial utilization strategies coupled with the augmentation in population density, additionally, soaring property prices have curtailed housing space. This metric underscores the complex relationship between urbanization and individual spatial needs, informing sustainable urban planning approaches.

Table 8. The Outcome Metrics Emanating From Indicator SDG 11.3.1 Throughout The Studied Timeframe

Period	Absolute change of built-up area (Km2)	Total change in built up area (%)	Land Consumption Rate (LCR)	Absolute change of population	Population Growth rate (PGR)	LCRPGR
1994 - 2004	+11.00	76.98%	+0.077	+84655	+0.029	+2.64
2004 - 2014	+11.97	47.33%	+0.047	+78180	+0.021	+2.25
2014 - 2022	+4.40	11.81%	+0.015	+78182	+0.022	+0.68

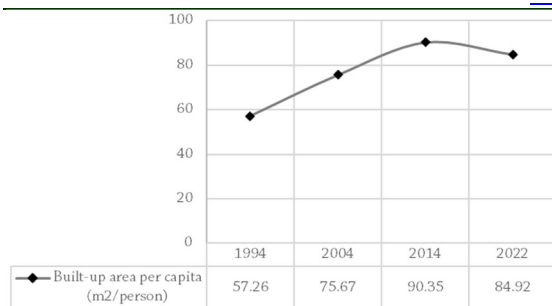


Figure 10. Built-Up Area Per Capita Trend Throughout The Studied Timeframe.

## 5. CONCLUSION AND PERSPECTIVES

The present study has conducted a thorough analysis of SDG Indicator 11.3.1 and the evolving urban dynamics within Kenitra city, employing medium spatial resolution satellite imagery to map built-up areas and a 28-year span population grid.

Quantifying land consumption per capita and assessing changes in the built-up area, in conjunction with SDG Indicator 11.3.1, provides an essential perspective on Kenitra's urban advancement pace and trajectory. These findings offer invaluable insights for achieving sustainable development goals, enhancing our understanding of evolving trends and how to address fundamental service requirements. This approach helps prevent potential disparities compared to other urban areas, aiding in well-informed policy formulation. Therefore, these insights aid in crafting strategies to promote optimal land utilization, preserving the natural environment and crucial agricultural spaces.

While the study's strength lies in the use of Landsat images, it faces a specific limitation due to the 30-meter resolution, which may not fully support comprehensive urban expansion analyses. However, the consistent availability of these images across all study periods stands as a crucial advantage, offering a reliable source of imagery, ensuring consistency in various classification outcomes, and effectively tracking urban expansion changes over time.

The two principal components employed for measuring indicator 11.3.1, meticulously crafted, possess extensive versatility and generic applications, extending their utility to estimating a spectrum of other indicators. The primary component prioritizes the creation of a finely detailed population matrix, specifically tailored to the distinctive requisites of select indicators, such as Dasymeric Population Mapping. Meanwhile, the

secondary component maximizes the potential of cloud computing and advanced artificial intelligence methodologies to harness insights from openly accessible satellite imagery, targeting diverse land cover categorizations. These technical advancements are purposed to notably enhance the precision and reliability of SDG indicators, thereby fortifying the integrity and robustness of the assessments.

The study's focus is Kenitra city, primarily serving as an experimental endeavor aimed at rigorously assessing and validating the chosen methodology. The overarching goal remains the nationwide application of this methodology across diverse urban agglomerations. This phase serves as a foundational test, affirming the efficacy and viability of the workflows used in this study. This experience significantly strengthens our confidence in the selected methodologies. Presently, we are actively implementing these refined methods across varied urban landscapes, striving to comprehensively calculate all SDG indicators.

## ACKNOWLEDGMENT

Many thanks to all those who contributed to the achievement of this research

## REFERENCES

- [1] Ibrahim M. Ramadan, and Manal A. Abdelfattah, "A proposed Model for enhancing e-government services to achieve sustainable development goals in EGYPT Case Study", *Journal of Theoretical and Applied Information Technology (JATIT)*, Vol. 100, No. 01, 2022, pp. 268-285, ISSN 1992-8645
- [2] High Commission for Planning (HCP), SDGs Platform <plateforme-odd.hcp.ma> last accessed 20/08/2023
- [3] United Nations, Department of Economic and Social Affairs, Sustainable Development <<https://sdgs.un.org/goals/goal11>>, last accessed 20/08/2023
- [4] Sanchez Rodriguez, R., Ürge-Vorsatz, D. & Barau, A.S. Sustainable Development Goals and climate change adaptation in cities. *Nature Clim Change* 8, 181–183 (2018). <https://doi.org/10.1038/s41558-018-0098-9>
- [5] E. Elbrirchi, I. Hbiak, "Measuring public transport accessibility in Casablanca according to united nations sustainable development goals using a geographical information system", *Journal of Theoretical and Applied*

- Information Technology (JATIT) 15th November 2022 -- Vol. 100. No. 21-- 2022
- [6] A recommendation on the method to delineate cities, urban and rural areas for international statistical comparisons. <<https://unstats.un.org/unsd/statcom/51st-session/documents/BG-Item3j-RecommendationE.pdf>>, last accessed 20/08/2023
- [7] UN-Habitat. SDG Indicator 11.3.1 Training Module: Land Use Efficiency; UN-Habitat: Nairobi, Kenya, 2018
- [8] Adel Shalaby, Ryutaro Tateishi, Remote sensing and GIS for mapping and monitoring land cover and land-use changes in the Northwestern coastal zone of Egypt, Applied Geography, Volume 27, Issue 1, 2007, Pages 28-41, ISSN 0143-6228, <https://doi.org/10.1016/j.apgeog.2006.09.004>.
- [9] Bardan Ghimire, John Rogan, Víctor Rodríguez Galiano, Prajjwal Panday & Neeti Neeti (2012) An Evaluation of Bagging, Boosting, and Random Forests for Land-Cover Classification in Cape Cod, Massachusetts, USA, GIScience & Remote Sensing, 49:5, 623-643, DOI: 10.2747/1548-1603.49.5.623
- [10] Cory L. Eicher & Cynthia A. Brewer (2001) Dasyetric Mapping and Areal Interpolation: Implementation and Evaluation, Cartography and Geographic Information Science, 28:2, 125-138, DOI: 10.1559/152304001782173727
- [11] Le Yu, Lu Liang, Jie Wang, Yuanyuan Zhao, Qu Cheng, Luanyun Hu, Shuang Liu, Liang Yu, Xiaoyi Wang, Peng Zhu, Xueyan Li, Yue Xu, Congcong Li, Wei Fu, Xuecao Li, Wenyu Li, Caixia Liu, Na Cong, Han Zhang, Fangdi Sun, Xinfang Bi, Qinchuan Xin, Dandan Li, Donghui Yan, Zhiliang Zhu, Michael F. Goodchild & Peng Gong (2014) Meta-discoversies from a synthesis of satellite-based land-cover mapping research, International Journal of Remote Sensing, 35:13, 4573-4588, DOI: 10.1080/01431161.2014.930206
- [12] T. Nery, R. Sadler, M. Solis-Aulestia, B. White, M. Polyakov and M. Chalakh, "Comparing supervised algorithms in Land Use and Land Cover classification of a Landsat time-series," 2016 IEEE International Geoscience and Remote Sensing Symposium (IGARSS), 2016, pp. 5165-5168, doi: 10.1109/IGARSS.2016.7730346.
- [13] Talukdar, Swapan, Pankaj Singha, Susanta Mahato, Shahfahad, Swades Pal, Yuei-An Liou, and Atiqur Rahman. 2020. "Land-Use Land-Cover Classification by Machine Learning Classifiers for Satellite Observations—A Review" Remote Sensing 12, no. 7: 1135. <https://doi.org/10.3390/rs12071135>
- [14] Thanh Noi, Phan, and Martin Kappas. 2018. "Comparison of Random Forest, k-Nearest Neighbor, and Support Vector Machine Classifiers for Land Cover Classification Using Sentinel-2 Imagery" Sensors 18, no. 1: 18. <https://doi.org/10.3390/s18010018>
- [15] Shelestov Andrii, Lavreniuk Mykola, Kussul Nataliia, Novikov Alexei, Skakun Sergii, "Exploring Google Earth Engine Platform for Big Data Processing: Classification of Multi-Temporal Satellite Imagery for Crop Mapping", Frontiers in Earth Science, 5, 2017, DOI:10.3389/feart.2017.00017
- [16] A Huete, K Didan, T Miura, E.P Rodriguez, X Gao, L.G Ferreira, Overview of the radiometric and biophysical performance of the MODIS vegetation indices, Remote Sensing of Environment, Volume 83, Issues 1–2, 2002, Pages 195-213, ISSN 0034-4257, [https://doi.org/10.1016/S0034-4257\(02\)00096-2](https://doi.org/10.1016/S0034-4257(02)00096-2).
- [17] A.R Huete, A soil-adjusted vegetation index (SAVI), Remote Sensing of Environment, Volume 25, Issue 3, 1988, Pages 295-309, ISSN 0034-4257, [https://doi.org/10.1016/0034-4257\(88\)90106-X](https://doi.org/10.1016/0034-4257(88)90106-X).
- [18] Russell G. Congalton, A review of assessing the accuracy of classifications of remotely sensed data, Remote Sensing of Environment, Volume 37, Issue 1, 1991, Pages 35-46, ISSN 0034-4257, [https://doi.org/10.1016/0034-4257\(91\)90048-B](https://doi.org/10.1016/0034-4257(91)90048-B).
- [19] United Nations, Department of Economic and Social Affairs, Statistics Division, SDG Indicator 11.3.1 Metadata <<https://unstats.un.org/sdgs/metadata/files/Metadata-11-03-01.pdf>>, last accessed 20/08/2023
- [20] Atlas of Urban Expansion <<http://atlasofurbanexpansion.org/about>>, last accessed 2023/06/18
- [21] Atlas of Urban Expansion, Understanding and Measuring Urban Expansion <[http://atlasofurbanexpansion.org/file-manager/userfiles/data\\_page/Methodology/Understanding\\_and\\_Measuring\\_Urban\\_Expansion.pdf?time=1476446554646](http://atlasofurbanexpansion.org/file-manager/userfiles/data_page/Methodology/Understanding_and_Measuring_Urban_Expansion.pdf?time=1476446554646)>, last accessed 20/08/2023
- [22] Lloyd, C., Sorichetta, A. & Tatem, A. High resolution global gridded data for use in

- population studies. *Sci Data* 4, 170001 (2017).  
<https://doi.org/10.1038/sdata.2017.1>
- [23] Leyk, S., Gaughan, A. E., Adamo, S. B., de Sherbinin, A., Balk, D., Freire, S., Rose, A., Stevens, F. R., Blankespoor, B., Frye, C., Comenetz, J., Sorichetta, A., MacManus, K., Pistolesi, L., Levy, M., Tatem, A. J., and Pesaresi, M.: The spatial allocation of population: a review of large-scale gridded population data products and their fitness for use, *Earth Syst. Sci. Data*, 11, 1385–1409, <https://doi.org/10.5194/essd-11-1385-2019>, 2019.
- [24] Nieves JJ, Stevens FR, Gaughan AE, Linard C, Sorichetta A, Hornby G, Patel NN, Tatem AJ. Examining the correlates and drivers of human population distributions across low- and middle-income countries. *J R Soc Interface*. 2017 Dec;14(137):20170401. doi: 10.1098/rsif.2017.0401. PMID: 29237823; PMCID: PMC5746564.
- [25] Melchiorri, M.; Pesaresi, M.; Florczyk, A.J.; Corbane, C.; Kemper, T. Principles and Applications of the Global Human Settlement Layer as Baseline for the Land Use Efficiency Indicator—SDG 11.3.1. *ISPRS Int. J. Geo Inf.* 2019, 8, 96.
- [26] Corbane, C.; Politis, P.; Siragusa, A.; Kemper, T.; Pesaresi, M. Estimation of Land Use Efficiency from the Global Human Settlement Layer (GHSL); A tool to Calculate the Land Use; Publications Office of the European Union: Luxembourg, 2018.
- [27] UN-Habitat. Metadata on SDGs Indicator 11.3.1. UN Habitat: Nairobi, Kenya, 2016
- [28] Database of indicators from the 2014 General Population and Housing Census in tabular form <[rgphentableaux.hcp.ma](http://rgphentableaux.hcp.ma)>, last accessed 20/08/2023
- [29] Database of indicators from the 2004 General Population and Housing Census <<https://applications-web.hcp.ma/hpmc/frmmarocenchiffres.aspx>>, last accessed 20/08/2023